2

The interaction of energetic solar photons with the upper atmosphere

The major neutral molecular constituents in the thermosphere, N_2 and O_2, are a legacy of the evolution of the Earth's atmosphere, and the present day abundance is controlled largely by geochemical and biological processes, as is the concentration of the minor molecular species, CO_2. The major atomic constituent, O, is produced from dissociation of O_2 by solar UV photons and by energetic particle impact. These processes also account for the presence of N atoms. The minor species NO, O_3 and OH result from chemical reactions, while H_2O, He, H_2, Ar, CH_4 and CO_2 are transported into the thermosphere from the mesosphere and lower levels of the atmosphere.

All the charged species that make up the ionosphere are produced either directly by photoionization and impact ionization of neutral atoms and molecules, or indirectly by subsequent ionic–chemical reactions. Photodetachment rapidly destroys any negative ions that may be formed in the thermosphere and the ionic population consists of several species of positive ions and an electron density equal to the sum of the positive ion densities.

In this chapter we compute the direct production rates of O and N atoms, and of the ions N_2^+, O_2^+, N^+ and O^+ by energetic photons. This requires knowledge of the energy distribution of the solar UV intensity, various cross sections (defined in Chapter 4), and densities of the major molecular species. Electronically excited states of atoms, molecules and ions will be treated because excited states play a major role in chemical reactions, spectroscopic emissions, and the energy balance in the thermosphere.

2.1 The solar irradiance

The transfer of solar radiation in the atmosphere does not involve emission sources or scattering into the original beam (with some important exceptions that are taken up in Chapter 7), and the process is well described by the Lambert–Beer exponential absorption law,

$$I(\lambda) = I_\infty(\lambda) \exp[-\tau(\lambda)] \tag{2.1.1}$$

At any point in the atmosphere the intensity at wavelength λ is $I(\lambda)$ and $\tau(\lambda)$ is the optical depth. In this section we focus on the irradiance at 1 AU 'at the top of the

atmosphere', i.e., $I_\infty(\lambda)$. The optical depth will be taken up in Section 2.2.

The wavelength region with which we concern ourselves is the UV portion of the solar spectrum which is absorbed in the atmosphere above about 80 km. Space borne instruments are therefore required to measure the radiation and this has only become possible since the advent of rocket and satellite technology. Solar UV irradiance measurements extend over solar cycle 20 and, to date, about half of cycle 21. Measurements made with instruments carried on board satellites yield data over extended periods of time but the inability to perform in-flight calibration and the inevitable degradation of detectors lead to uncertainties in both absolute and relative values of the irradiance at different wavelengths. Rocket borne instruments yield snapshots of the solar irradiance, but less than two dozen measurements have been made since 1960, most experiments covering only a limited wavelength interval. Even the limited data sets that have been obtained clearly show considerable variability in the UV spectral intensities, with the magnitude of the variability related to other variable solar parameters such as the decametric radiation, cyclical variations, and flare activity.

The solar UV spectrum between 14 Å and 2000 Å obtained on 23 April 1974 is shown in Figure 2.1.1. The wavelength resolution is 1 Å and the flux magnitude, usually specified in units of photons $cm^{-2} s^{-1} Å^{-1}$, is just photons $cm^{-2} s^{-1}$ in this case. This

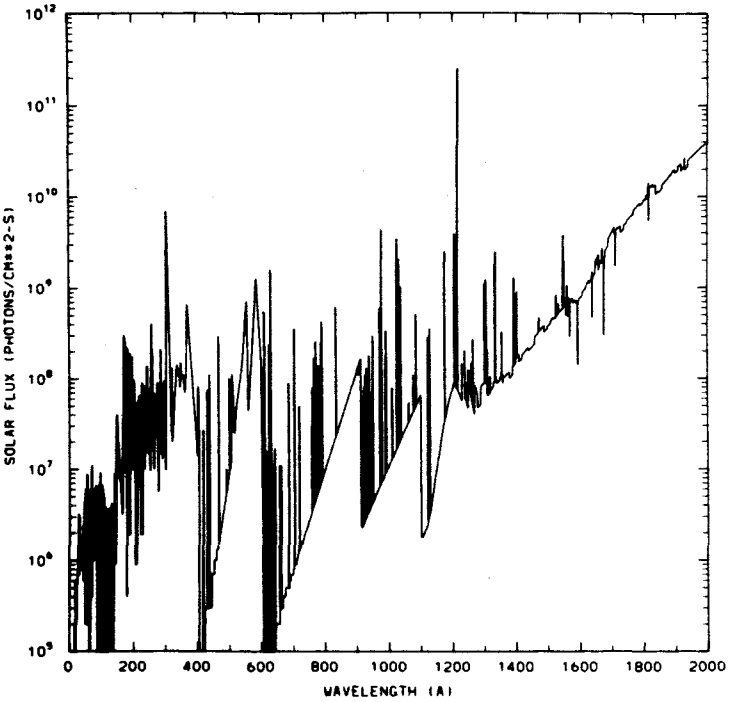

Fig. 2.1.1 Solar UV flux measured on 23 April 1974 at 1 Å intervals. This is the aeronomical reference spectrum F74113 for the Atmosphere Explorer satellite solar flux measurements. (R.G. Roble and B.A. Emery, *Planet. Space Sci.*, **31**, 597, 1983.)

https://doi.org/10.1017/CBO9780511573118.003 Published online by Cambridge University Press

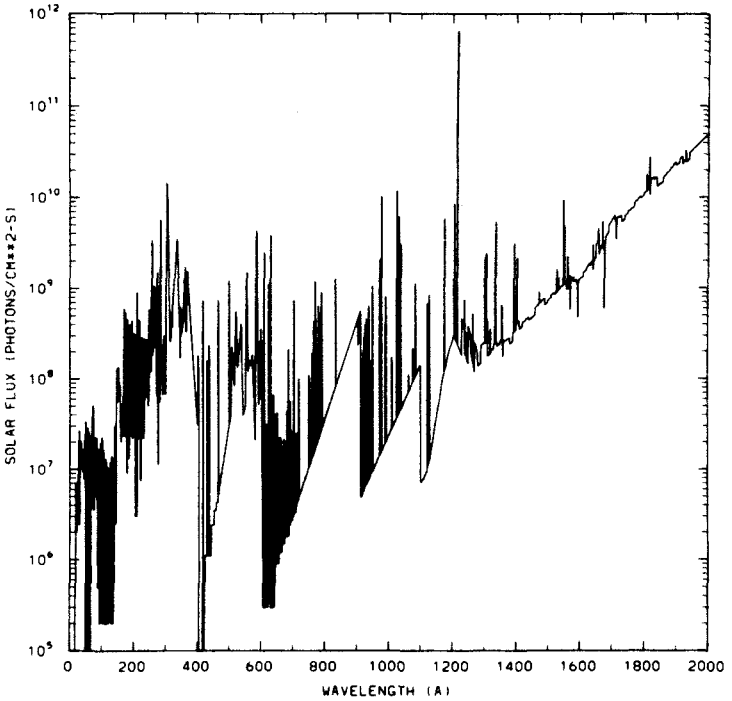

Fig. 2.1.2 Solar UV flux measured on 19 February 1979 at 1 Å intervals. (R.G. Roble and B.A. Emery, *Planet. Space Sci.*, **31**, 597, 1983.)

is an important spectrum because it served as a calibration spectrum for the spectrometers carried by the Atmosphere Explorer satellites between 1974 and 1981. The April 1974 epoch is representative of solar minimum activity. Figure 2.1.2 shows a similar spectrum obtained five years later during the maximum of the solar activity cycle. A brief period in July 1976, during which there were essentially no sunspots on the disc, is adopted as representative of minimum solar UV irradiance. The ratio of the solar UV flux obtained on 19 February 1979 to the July 1976 minimum is shown in Figure 2.1.3. The solar UV irradiance spectrum is a composite of many emission lines and continua (Problem 1). The flux varies over many orders of magnitude in the wavelength interval that contributes to thermospheric and ionospheric processes. Flux variability between solar maximum and solar minimum conditions strongly depends on wavelength. Variability is largest at the short wavelengths consisting of emission from the hottest region of the solar atmosphere, the corona and the upper chromosphere. Large increases of irradiance are associated with solar flares. Geophysical parameters associated with the April 1974, July 1976 and February 1979 periods are summarized in Table 2.1.1.

The pictorial presentation of the solar UV irradiance (Figures 2.1.1–2.1.3) provides a good overview of the wavelength dependence of this input parameter. However, for computations it is more convenient to present the measurements in tabular form and to combine photon intensities into larger wavelength intervals. Intensities of the brighter

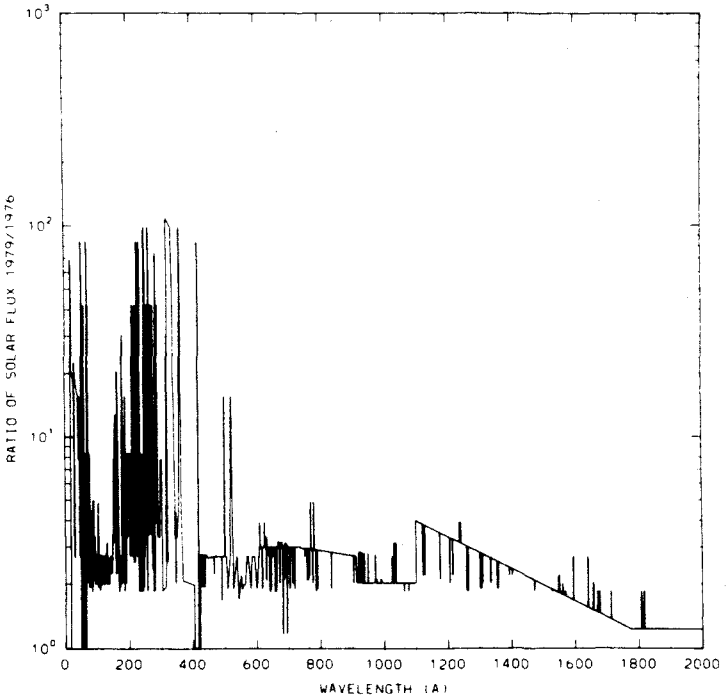

Fig. 2.1.3 Ratio of solar UV intensities measured on 19 February 1979 to the observations obtained during July 1976 on days of spotless solar conditions. (R.G. Roble and B.A. Emery, *Planet. Space Sci.*, **31**, 597, 1983.)

Table 2.1.1 *Geophysical parameters for various periods*

Day	F 10.7	$\overline{\text{F 10.7}}$	E_f	A_p	K_p
23 April 1974	74.5	86.1	1.99	29	5^- 4^- 4^- 5 4^- 4^- 4^-
13–28 July 1976	66.4–69.1	71.8	2.07	3–19	1^- 1^- 0 1^- 2^- 1^- 0 (21st)
(average = 67.6)			(average = 7 (15th))		2^- 2^- 2 2 2^- 4^+ 6^- 4^-
19 February 1979	243.3	187.7	7.19	15	4^+ 3 3^+ 2^+ 4 2^+ 3^+ 2

$\overline{\text{F 10.7}}$ – the 10.7 cm radiowave flux from the sun in units of ($\times 10^{-22}$ W m^{-2} Hz^{-1}) for the previous day.
F 10.7 – the 3 month solar rotation average of the F 10.7 solar flux centred on the day indicated.
E_f = solar UV energy flux in erg cm^{-2} s^{-1} integrated in wavelength from 14.25 to 1017 Å.
A_p = daily planetary geomagnetic index.
K_p = three hourly values of the planetary magnetic index on a quasi-logarithmic scale ranging from 0 to 9^+.

emission lines are still listed separately. One such tabulation is shown in Appendix 2 for five representative days in solar cycle 20. The wavelength range between 50 and 1050 Å includes the ionization energy of all major atomic and molecular constituents of the thermosphere (Section 2.3). Longer wavelength photons are capable of dissociating O_2 molecules, as well as other species; this will be discussed in Section 2.4. The reference

spectrum in the wavelength range between 1050 and 1940 Å is listed in Appendix 2. Considerable variability of the solar irradiance is still found in this wavelength region, as shown in Figure 2.1.3.

2.2 The optical depth

The optical depth, $\tau(\lambda)$, a parameter that appears in the Lambert–Beer law (Equation (2.1.1)), specifies the attenuation of the solar irradiance by the atmosphere. For a vertical sun, and at altitude z_0 it is, simply,

$$\tau^{v}_{z_0}(\lambda) = \sum_j \sigma^{a}_j(\lambda) \int_{z_0}^{\infty} n_j(z)\,dz \tag{2.2.1}$$

where the $\sigma^{a}_j(\lambda)$s are the wavelength-dependent absorption cross sections of species j and the $n_j(z)$s are the height profiles of their concentrations. For a slant path on a spherical earth the equation is slightly more complex. Figure 2.2.1 illustrates the geometry for solar zenith angles χ_0 less than 90° and greater than 90°. The earth's radius is R, the altitude at which the photon flux is evaluated is z_0, and z_s is a screening height below which the atmosphere is essentially opaque to photons of wavelength λ. For the $\chi_0 < 90°$ case,

$$\frac{\sin\chi}{R+z_0} = \frac{\sin\chi_0}{R+z} \tag{2.2.2}$$

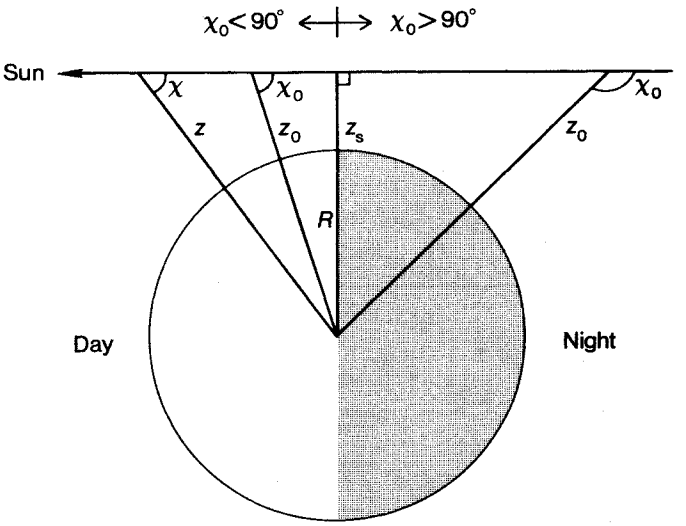

Fig. 2.2.1 Geometry adopted for computing the attenuation of solar irradiance (not to scale).

https://doi.org/10.1017/CBO9780511573118.003 Published online by Cambridge University Press

from which

$$\sec\chi = \left[1 - \left(\frac{R+z_0}{R+z}\right)^2 \sin^2\chi_0\right]^{-1/2} \tag{2.2.3}$$

and the optical depth is

$$\tau(\lambda, \chi_0, z_0) = \sum_j \sigma_j^a(\lambda) \int_{z_0}^{\infty} n_j(z)\left[1 - \left(\frac{R+z_0}{R+z}\right)^2 \sin^2\chi_0\right]^{-1/2} dz \tag{2.2.4}$$

Substantial effort has been devoted in the past toward expressing the integral by some analytic function, generically known as the Chapman function, or in tabular form. This hardly seems necessary any longer considering the ease of obtaining a solution numerically using a computer. For a solar zenith angle χ_0 less than about 75° it is found that $\sec\chi \approx \sec\chi_0$ for values of z_0 corresponding to ionospheric levels. The integral must still be retained if the altitude profiles of the concentrations of various species are arbitrary and not expressed in some analytic form.

For a solar zenith angle $\chi_0 > 90°$ the optical depth is

$$\tau(\lambda, z_0, \chi_0) = \sum_j \sigma_j^a(\lambda)\left\{2\int_{z_s}^{\infty} n_j(z)\left[1 - \left(\frac{R+z_s}{R+z}\right)^2\right]^{-1/2} dz - \int_{z_0}^{\infty} n_j(z)\left[1 - \left(\frac{R+z_0}{R+z}\right)^2 \sin^2\chi_0\right]^{-1/2} dz\right\} \tag{2.2.5}$$

The derivation is left as a problem (Problem 2). When $\chi_0 = 90°$ Equation (2.2.5) reduces to Equation (2.2.4) since $z_0 = z_s$, and for $\chi_0 = 0°$, an overhead sun, both Equation (2.2.4) and Equation (2.2.5) reduce to Equation (2.2.1).

The altitude dependence of the concentrations of the major thermospheric neutral species (together with the temperature profile) is known as a neutral atmosphere model. Several empirical models have been developed based on measurements obtained over long periods of time, a range of altitudes, latitudes, longitudes and levels of 'solar activity'. One goal of upper atmosphere research has been, and still is, to test our ability to model the response of the thermosphere and ionosphere to various inputs, such as a variable solar irradiance, i.e., to predict the changes in density, composition, temperature, etc. that are observed. Here we are faced with a dilemma. We must assume a model atmosphere to compute the optical depth which then enables us to derive the solar flux as a function of altitude and the multitude of effects that it has on the atmosphere. Among these effects will be changes in the model parameters that were assumed to begin the process. Moreover, rocket and satellite borne instruments do not measure the solar irradiance at the 'top of the atmosphere'; instead, $I(\lambda)$ is measured over a range of altitudes. To infer $I_\infty(\lambda)$ from the measurements a model atmosphere must be assumed. This interdependence of physical parameters is characteristic of the system being studied, the upper atmosphere, and we will be faced with similar situations throughout this book. Appendix 1 is devoted to empirical neutral atmosphere models.

The remaining parameter in the expression for the optical depth is the absorption cross section. The photoabsorption cross sections for the major thermospheric species are shown in Figures 2.2.2–2.2.4. The wavelength region relevant to our purpose, computing ionization and dissociation rates, is determined by the following related

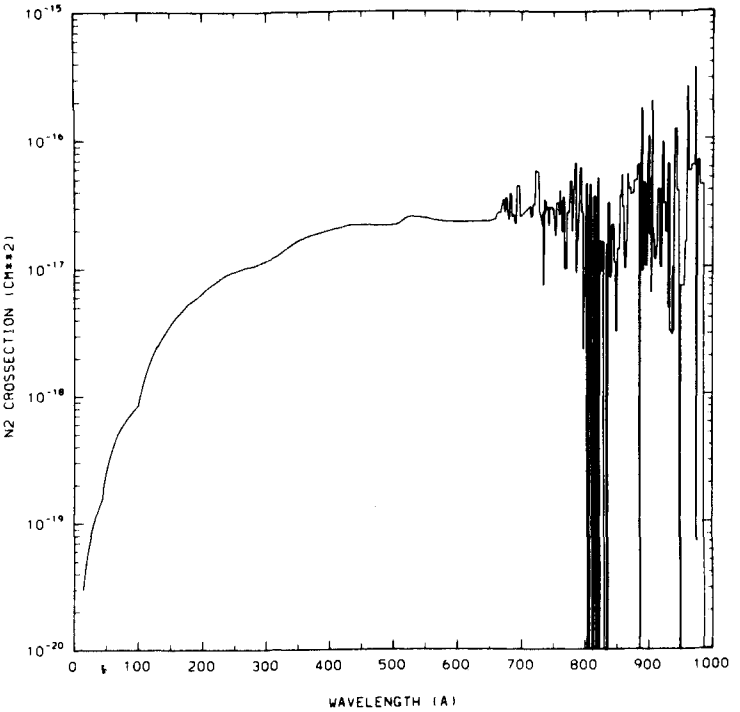

Fig. 2.2.2 Absorption cross sections for N_2. (R.G. Roble and B.A. Emery, *Planet. Space Sci.*, **31**, 597, 1983.)

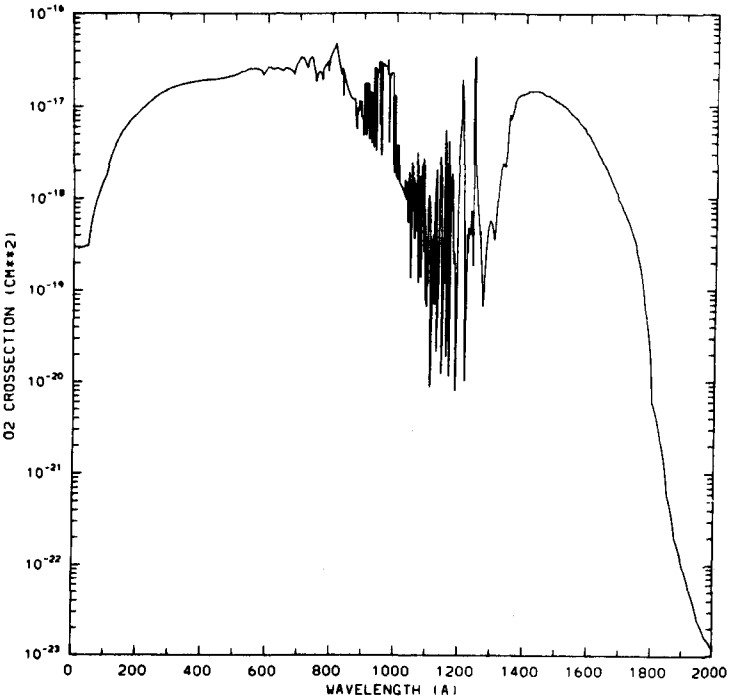

Fig. 2.2.3 Absorption cross sections for O_2. (R.G. Roble and B.A. Emery, *Planet. Space Sci.*, **31**, 597, 1983.)

https://doi.org/10.1017/CBO9780511573118.003 Published online by Cambridge University Press

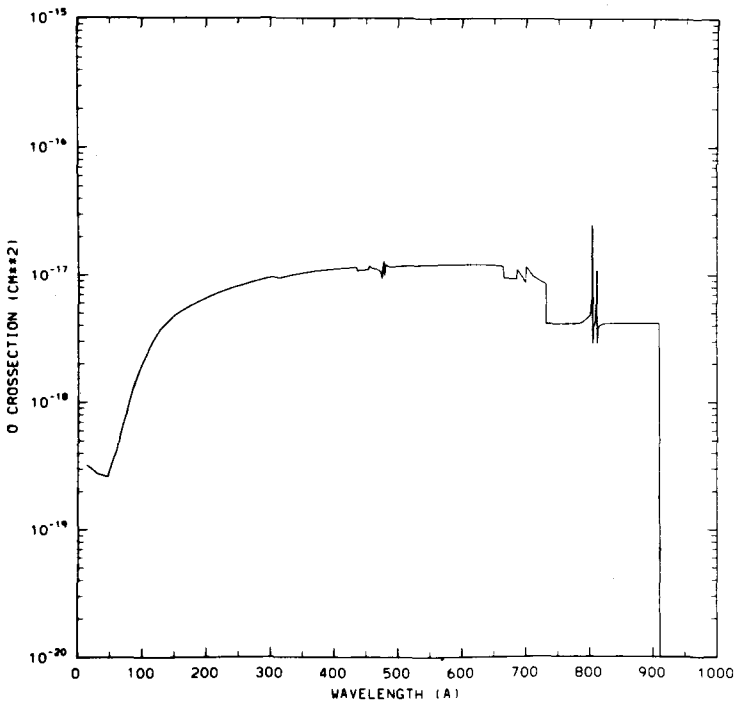

Fig. 2.2.4 Absorption cross sections for O. (R.G. Roble and B.A. Emery, *Planet. Space Sci.*, **31**, 597, 1983.)

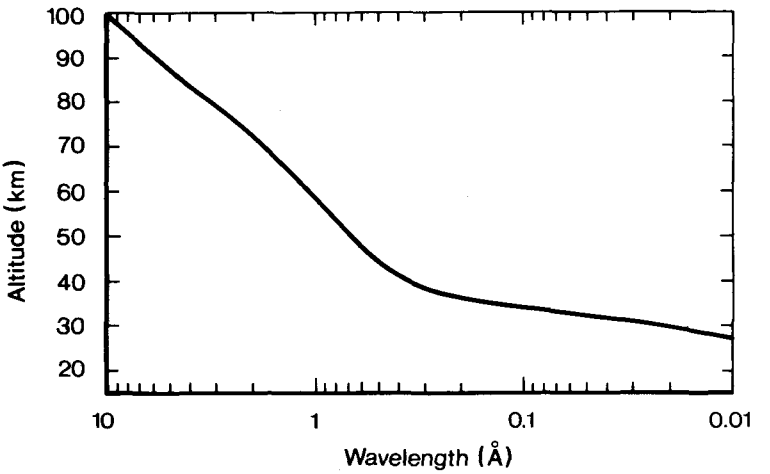

Fig. 2.2.5 Altitudes of the unit optical depth for $0.01 \leqslant \lambda \leqslant 10$ Å.

https://doi.org/10.1017/CBO9780511573118.003 Published online by Cambridge University Press

Table 2.2.1 *Ionization and dissociation threshold energies and wavelengths*

	Ionization		Dissociation	
Species	(eV)	λ(Å)	(eV)	λ(Å)
N_2	15.58	796	9.76	1270
O_2	12.08	1026	5.12	2422
O	13.61	911		
N	14.54	853		
NO	9.25	1340	6.51	1905
H	13.59	912		
He	24.58	504		

considerations. The photons must be absorbed in the thermosphere. This implies an absorption cross section which is of the order of magnitude of the inverse of the column density of the absorbing species above the lowest height level of interest, about 90 km, resulting in approximately unit vertical optical depth (Problem 3). Figure 2.2.5 shows the altitude of unit optical depth for X-rays in the wavelength region between 0.01 and 10 Å. The photon energy must also exceed the threshold energy for ionization and/or dissociation of the neutral constituents. Table 2.2.1 presents these thresholds for the thermospheric and ionospheric species. Absorption cross sections are given in tabular form in Appendix 2. Examination of the curves in Figures 2.2.2–2.2.4 shows that in the wavelength region of the continua the absorption cross section varies relatively smoothly with wavelength but that molecular band absorption is highly structured. In the region between the Schumann–Runge continuum and the photoionization limit ($\sim$ 1350–1026 Å) in O_2 especially large changes in the magnitude of the cross section occur, varying by three powers of ten within a range of a few ångstroms. Fortuitously, there is a deep minimum in the absorption cross section ($\sim 1 \times 10^{-20}$ cm^2) at the wavelength of the H Lyman alpha (H-Ly-α) solar emission line ($\sim$ 1215.7 Å) which has a large and variable intensity (Figure 2.2.6). Since this wavelength region lies beyond the absorption edge of O and N_2, only O_2 need be included in computing the optical depth at 1216 Å. Adopting the O_2 concentration given in Appendix 1 we find that unit optical depth for O_2 is at a level of about 85 km. It would therefore seem that the H-Ly-α radiation should pass right through the thermosphere. This would indeed occur were it not for the minor constituent NO. The ionization threshold wavelength of NO is 1340 Å and the ionization cross section is large. Thus, thermospheric NO is efficiently ionized by H-Ly-α. The NO density, however, is insufficient to prevent most of the radiation from penetrating to the level of the mesosphere and becoming a major source of D-region ionization.

2.3 Photoionization

Photoionization is the principal mechanism that produces the ionosphere. For the three major thermospheric species we have

https://doi.org/10.1017/CBO9780511573118.003 Published online by Cambridge University Press

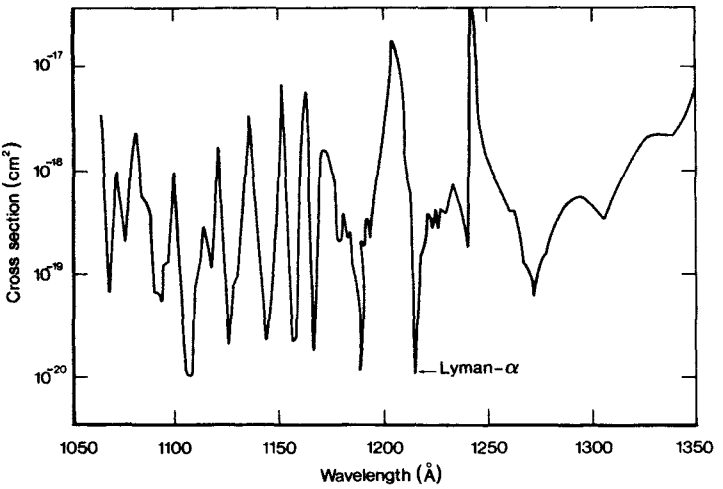

Fig. 2.2.6 Absorption cross sections of O_2 between 1050 and 1350 Å. (K. Watanabe, *Advances in Geophysics*, Eds. H.E. Landsberg and J. Van Mieghen, **5**, 153, 1958.)

$$N_2 + h\nu (< 796\,\text{Å}) \rightarrow N_2^+ + e \tag{2.3.1}$$

$$O_2 + h\nu (< 1026\,\text{Å}) \rightarrow O_2^+ + e \tag{2.3.2}$$

and

$$O + h\nu (< 911\,\text{Å}) \rightarrow O^+ + e \tag{2.3.3}$$

The wavelengths specified in Reactions (2.3.1)–(2.3.3) correspond to the ionization thresholds, λ_{th}, listed in Table 2.2.1 for the production of ions in their ground electronic state. The photoionization rate of species j at altitude z is

$$P_z^i(j,l) = n_z(j) \int_{\lambda_{th}}^{0} I_z(\lambda)\sigma_j^i(\lambda)p_j^i(\lambda,l)\,d\lambda \qquad (\text{ions cm}^{-3}\,\text{s}^{-1}) \tag{2.3.4}$$

Quantities not previously defined are the ionization cross section, $\sigma_j^i(\lambda)$, and the branching ratios $p_j^i(\lambda, l)$ that identify production of ions in various electronically excited states, l, or in the ground state. For each constituent,

$$\sum_j p_j^i(\lambda, l) = 1 \tag{2.3.5}$$

The integration in Equation (2.3.4) is carried from the ionization threshold wavelength, λ_{th}, to the shortest wavelength (not zero, as has been shown) at which the photon flux is sufficient to contribute to ion production. X-ray photons of wavelength shorter than about 10 Å are absorbed largely below 100 km (Figure 2.2.5). The photon flux is small but highly variable.

Dissociative ionization is an additional source of atomic ions,

$$O_2 + h\nu (< 662\,\text{Å}) \rightarrow O^+ + O + e \tag{2.3.6}$$

and

$$N_2 + h\nu (< 510\,\text{Å}) \rightarrow N^+ + N + e \tag{2.3.7}$$

Photons with sufficient energy to both ionize and dissociate the molecule are required.

https://doi.org/10.1017/CBO9780511573118.003 Published online by Cambridge University Press

The threshold wavelengths for reactions specified up to this point are valid for the formation of ions in the ground state. A substantial fraction of ions and neutrals in the thermosphere is produced in electronically excited states and with an enhanced vibrational population distribution, though the latter not by photon impact. Various consequences of the formation of excited states will be discussed in this and succeeding chapters. An overview of the various states associated with each of the major thermospheric species is best obtained from the energy level diagram for each species. Simplified diagrams showing the excited states of N_2^+, O_2^+ and O^+ relevant to the present subject are given in Figure 2.3.1. Complete energy level diagrams for atoms and atomic ions and potential curves as a function of internuclear distance for molecules and molecular ions are presented in Appendix 3; frequent reference will be made to these diagrams. The contribution of double or multiple ionization is too small to warrant inclusion here.

Cross sections for ionization of O leading to different electronic states of the ion have been computed theoretically. For the molecular ions, however, it is difficult both theoretically and experimentally to determine cross sections for each excited ionic state. It has been common practice to specify the total photoionization cross section, $\sigma_j^i(\lambda)$, and the branching ratios, $p_j^i(\lambda, l)$, using compatible wavelength intervals. The different states of the ions are shown in Figure 2.3.1, including the respective threshold energies. The total photoionization cross sections and branching ratios are given in

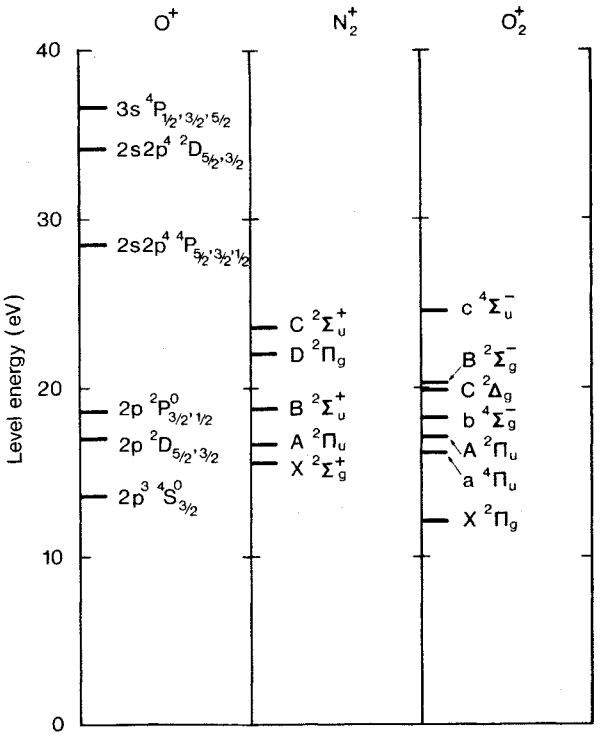

Fig. 2.3.1 Partial energy level diagrams of the major ionizable thermospheric species. The lowest level corresponds to the ionization energy of the neutral species.

https://doi.org/10.1017/CBO9780511573118.003 Published online by Cambridge University Press

Appendix 2, as is the fraction of ionization events going into dissociative ionization. For computational convenience the same wavelength intervals are adopted that have been used for the solar irradiance spectrum and for the absorption cross sections. We will learn in Chapter 7 how several excited states produced by photoionization lead to optical emissions that are part of the dayglow spectrum (Problem 4).

2.4 Photodissociation

Photodissociation of O_2 accounts for O being the major neutral species in the thermosphere above about 200 km. Two-body recombination is very slow so that O atoms must diffuse downward into the denser regions of the atmosphere where three-body recombination is the destruction mechanism, i.e., below approximately 100 km. The time constant for downward diffusion of O atoms is long compared with the diurnal cycle of solar illumination, preventing any significant night time decrease in the thermospheric abundance of O atoms.

The dissociation threshold energy of O_2 is only 5.12 eV (Table 2.2.1) so that photons at wavelengths less than 2422 Å are effective in the process

$$O_2 + h\nu(< 2422\,\text{Å}) \rightarrow O + O \tag{2.4.1}$$

However, solar irradiance beyond 1800 Å is absorbed below the thermosphere and most of the thermospheric dissociation of O_2 is caused by photons in the wavelength region of the Schumann Runge continuum. Taking account of the entire spectral range, the rate of photodissociation at altitude z is

$$P_z^{\mathrm{d}}(O_2) = n_z(O_2) \int_{2422\,\text{Å}}^{650\,\text{Å}} I_z(\lambda)\sigma_{O_2}^{\mathrm{d}}(\lambda)\,\mathrm{d}\lambda \quad (\mathrm{cm}^{-3}\,\mathrm{s}^{-1}) \tag{2.4.2}$$

where $\sigma_{O_2}^{\mathrm{d}}(\lambda)$ is the photodissociation cross section. The short wavelength limit of integration, 650 Å, corresponds to the photoionization limit, i.e., photon absorption leads almost entirely to ionization (Appendix 2).

In Section 2.3 we noted that photoionization leads to several electronically excited states of the ions. Photodissociation likewise can lead to excitation of the products.

$$O_2 + h\nu(< 1749\,\text{Å}) \rightarrow O(^1D) + O(^3P) \tag{2.4.3}$$

The excitation energy of the $O(^1D)$ state is 1.97 eV (see Appendix 3). We mentioned earlier that it is the solar irradiance at wavelengths less than of about 1800 Å that is absorbed by O_2 in the thermosphere. Photodissociation of O_2 in the thermosphere is therefore a copious source of excited O atoms. This has important consequences which will be explored in succeeding chapters.

N_2 molecules also photodissociate. However, the process is quite different from dissociation of O_2 which occurs primarily by absorption of continuum radiation. N_2 molecules are first excited into several high lying valence and Rydberg states, called predissociation states which decay largely by dissociation of the molecule instead of by radiation. The absorption bands responsible for this process lie in the wavelength region between about 800 and 1000 Å (Fig. 2.2.2), i.e., just beyond the ionization threshold. Although not the major source of N in the thermosphere, photodissociation of N_2 via excitation of predissociation levels does contribute to the production of this minor constituent. It is generally assumed that the difference between the total

absorption cross section of N_2 and the ionization cross section (Appendix 2) is the effective dissociation cross section that may be used to compute the N atom production rate by an equation similar to Equation (2.4.2) (Problem 5). The predissociation mechanism is described in greater detail in Chapter 4 in connection with electron impact dissociation of N_2.

2.5 Photoelectrons

In our discussion of photoionization (Section 2.3) we indicated by Reactions (2.3.1)–(2.3.3) that the process leads to the production of ion–electron pairs, and this also applies to dissociative ionization, Reactions (2.3.6) and (2.3.7). The threshold wavelengths associated with each reaction specify the minimum photon energy that is required for the reaction to proceed; however, the photoionization cross section is larger at wavelengths shorter than the threshold wavelength (Appendix 2). The reactions, therefore, proceed at a higher rate in association with excess energy. As already mentioned, there is the probability (cross section) that the excess energy leads to internal excitation of the product ions (e.g., N_2^+ $A^2\Pi_u$, O_2^+ a $^4\Pi_u$, O^+ ^2D) but much of the excess energy is channelled into kinetic (translational) energy of the products. Momentum conservation shows that most of the energy is imparted to the lighter electrons. Photoionization, therefore, is a source of energetic photoelectrons. The energy spectrum of photoelectron production is governed by the UV photon flux, a multitude of photoionization cross sections and the neutral gas composition of the atmosphere. The production rate of photoelectrons with energy E at altitude z is given by

$$P_z^e(E) = \sum_j \sum_l \sum_\lambda n_z(j)\sigma_j^i(\lambda)p_j^i(l, \lambda_{th}, \lambda)I_z(\lambda) \qquad (\text{cm}^{-3}\,\text{s}^{-1}) \qquad (2.5.1)$$

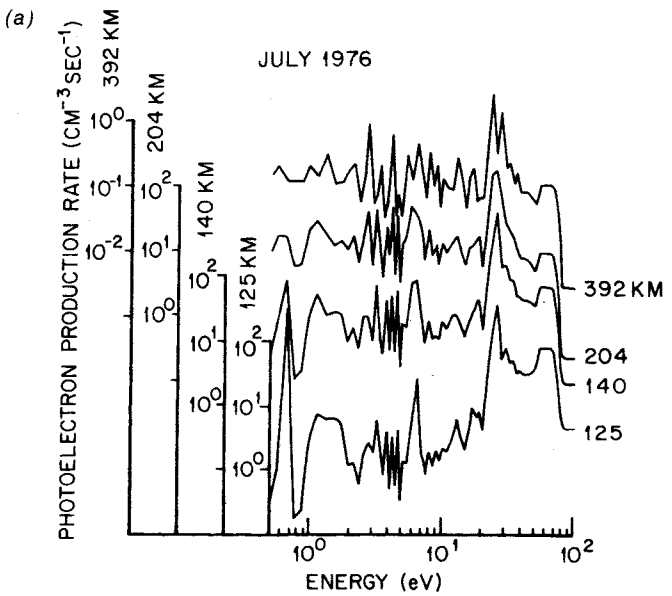

https://doi.org/10.1017/CBO9780511573118.003 Published online by Cambridge University Press

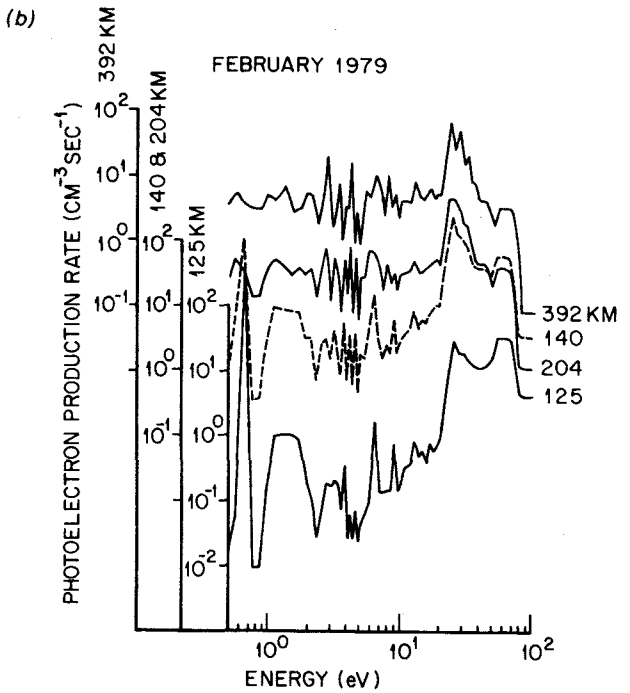

Fig. 2.5.1 The production rate of photoelectrons for typical solar minimum (*a*) and solar maximum (*b*) conditions as a function of electron energy at selected altitudes.

The electron energy will henceforth be specified in energy units, with

$$E = hc(1/\lambda_{th}(j,l) - 1/\lambda) \text{ (eV)} \tag{2.5.2}$$

Planck's constant is h and c is the speed of light. The threshold wavelength (or energy) is a function of the electronic state, l, of species, j. As noted in Section 2.1, the intensity of solar irradiance, $I_z(\lambda)$, may be specified per angstrom (Figures 2.1.1 and 2.1.2) or in finite wavelength intervals (e.g. 50 Å) plus discrete emission lines, as in Appendix 2. The summation over λ in Equation (2.5.1) must be treated accordingly. The branching ratios and excitation thresholds for the electronic states of the three major species in the thermosphere are listed in Appendix 2, corresponding to the states shown in Figure 2.3.1. Variability in the solar irradiance, $I_\infty(\lambda)$, with solar activity results in a corresponding variation of the photoelectron production rate, $P_z^e(E)$ (Problem 6). The production rates of photoelectrons as a function of energy for solar minimum (July 1976) and solar maximum (February 1979) conditions are shown in Figure 2.5.1 at selected altitudes. The structure in these curves is a consequence of structure in the solar irradiance as a function of wavelength.

Bibliography

The solar UV irradiance is one of the fundamental parameters in an investigation of the upper atmosphere and considerable effort has been expended in acquiring measurements of the

https://doi.org/10.1017/CBO9780511573118.003 Published online by Cambridge University Press

absolute fluxes and the variability with solar activity. A recent review paper evaluates published irradiance data from 1350 to 4000 Å:

P.C. Simon and G. Brasseur, Photodissociation effects of solar UV radiation, *Planet. Space Sci.*, **31**, pp. 987–99, 1983.

This paper also discusses the absorption cross section of O_2 which is required to interpret the flux measurements in the wavelength region considered in the review. Over eighty references are given to publications on the solar irradiance and absorption cross sections. The results of irradiance measurements obtained by many investigators over several years are compared, using as reference spectrum the one given in tabular form by

G. Brasseur and P.C. Simon, Stratospheric chemical and thermal response to long-term variability in solar UV irradiance, *J. Geophys. Res.*, **86**, 7343–62, 1981.

A critical evaluation of the solar irradiance between 140 and 1850 Å acquired by the Atmosphere Explorer satellites is given in the paper:

H.E. Hinteregger, K. Fukui, and B.R. Gilson, Observational, reference and model data on solar euv, from measurements on AE-E, *Geophys. Res. Lett.*, **8**, 1147–50, 1981.

This paper gives references to the sources of the measurements, specifically, the so-called reference spectrum acquired during a rocket flight:

L. Herox and H.E. Hinteregger, Aeronomical reference spectrum for solar UV below 2000 Å, *J. Geophys. Res.*, **83**, 5305, 1978.

The measurements on which the curves shown in Figures 2.1.2 and 2.1.3 are based are given in the paper

H.E. Hinteregger, Representations of solar EUV fluxes for aeronomical applications, *Adv. Space Res.*, **1**, 39, 1981.

Photoionization and photoabsorption cross sections in the wavelength region 34 Å to 1027 Å are given in a compilation of experimental and theoretical results by

K. Kirby–Docken, E.R. Constantinides, S. Babeu, M. Oppenheimer and G.A. Victor, Photoionization and photoabsorption cross sections of He, O, N_2 and O_2 for aeronomic calculations, *At. Data Nuclear, Data Tables*, **23**, 63–82, 1979.

The above data compilation also gives the branching ratios into excited states of O, N_2 and O_2 and the dissociative ionization yield for the molecular species. In the longer wavelength region absorption cross sections are summarized in the review article

K. Watanabe, Ultraviolet absorption processes in the upper atmosphere, *Adv. in Geophys.*, **5**, 153, 1958.

The density and composition of the neutral atmosphere may be specified by empirical models, based on very large data sets acquired by satellite borne instruments and ground based measurements. One such model includes data compiled over many years' observations, allowing for different levels of solar activity, magnetic activity, geographic and diurnal variations:

A.E Hedin, MSIS-86 thermospheric model, *J. Geophys. Res.*, **92**, 4649, 1986.

The above cited paper gives references to preceeding publications on empirical model atmospheres.

Problems 1–6

Problem 1 Identify some prominent line emissions in the solar spectra shown in Figures 2.1.1 and 2.1.2. Use the tables in Appendix 2 as well as the references. Which lines show large differences in intensity between solar minimum and maximum conditions?

Problem 2 Derive Equation (2.2.5) for the optical depth for solar zenith angles greater than 90°.

Problem 3 Compute the altitude at which $I(\lambda)$ is reduced to 1/e of the irradiance at the top of the atmosphere, $I_\infty(\lambda)$, as a function of wavelength for a solar zenith angle of 40°. Use the absorption cross sections in Appendix 2.

Problem 4 Compute the photoionization rate for solar maximum conditions when the solar zenith angle is 40°. Compute the altitude profiles of the production rate of various ions of the major thermospheric species. Assume that ions produced by dissociative ionization are formed in the ground state.

Problem 5 Compute the N atom production rate as a function of altitude by photodissociation of N_2 for solar maximum conditions and a solar zenith angle of 40°.

Problem 6 How much energy does a photoelectron acquire when produced by HeI photons ionizing N_2? Compute the photoelectron production rate due to the HeI and HeII solar emission lines at 170 km altitude for day 113 in 1974 and day 50 in 1979 for a solar zenith angle of 40°.

https://doi.org/10.1017/CBO9780511573118.003 Published online by Cambridge University Press